Review on Melt Flow Simulations for Thermoplastics and Their Fiber Reinforced Composites in Fused Deposition Modeling

Xuguang Xu[1], Huilin Ren[1], Shengyang Chen[3], Xiaofan Luo[4], Feihu Zhao[2*], Yi Xiong[1*]

[1] School of System Design and Intelligent Manufacturing, Southern University of Science and Technology, Shenzhen 518055, China

[2] Zienkiewicz Centre for Computational Engineering and Department of Biomedical Engineering, Faculty of Science and Engineering, Swansea University, Swansea SA1 8EN, United Kingdom

[3] INTAMSYS Technology Co., Ltd, Building E11, No.3188 Xiupu Road, 201315 Shanghai, Shanghai, China

[4] Polymaker LLC, 13223-A Stafford Rd, Missouri City, Texas 77489, USA

*Corresponding authors:
Yi Xiong, Email: xiongy3@sustech.edu.cn ;
Feihu Zhao, Email: feihu.zhao@swansea.ac.uk.

Abstract

Fused deposition modeling (FDM) has been one of the most widely used additive manufacturing techniques due to its ease of use and widespread availability. Recent years have witnessed a renaissance of research interest in FDM due to its rapid advances in creating high-performance and industrial-grade parts, e.g., fiber-reinforced polymer composites. Considerable efforts have been made to model the FDM process to reveal the underlying mechanisms that are not yet well understood. This study aims to provide a comprehensive review of recent progress on the melt flow simulations of polymers and their fiber-reinforced composites in FDM. Specifically, analytical and numerical methods for modeling the polymer melt flow in the extrusion and deposition are summarized and discussed. Additionally, the FDM process simulation for short and continuous fiber-reinforced polymer composites as an emerging research field is outlined and discussed. Finally, the outlook of future work on the numerical simulation of FDM is provided.

Keywords: Process simulation; Fused deposition modeling; Melt flow; Fiber-reinforced composites; Computational fluid dynamics

1. Introduction

Additive manufacturing (AM), also called three-dimensional (3D) printing, is a method based on computer-aided design (CAD) models to build complex parts by material addition in a layer-wise manner. Compared with conventional manufacturing techniques, AM provides more degrees of freedom in design and manufacturing to create high-performance, complex parts at low cost and high velocity. Due to continuous efforts, significant advances have been made to turn AM from rapid prototyping tools into a viable production option. Since the idea of AM was first introduced by Hull [1,2], various AM techniques have been developed, such as vat photopolymerization, material extrusion, binder jetting, material jetting, sheet lamination, powder bed fusion, and directed energy deposition [3].

Among these techniques, fused deposition modeling (FDM), or fused filament fabrication (FFF), has been one of the most widely used AM techniques due to its ease of use and widespread availability. As a material extrusion technique, the FDM machine feeds continuous filaments into a heated liquefier and deposits these melt flows through pressure onto a print bed to build up 3D objects. Early FDM machines are mainly at the desktop level and used for fabricating engineering thermoplastics, e.g., polylactic acid (PLA), thermoplastic polyurethane (TPU), and polyamide (PA). The applications of parts fabricated by these machines are limited due to their poor mechanical properties and geometry accuracy. For a long period, the industrial value of FDM has been heavily underrated, and less research attention has been given to this technology in contrast to other AM techniques. However, the emergence of several innovative FDM techniques for creating high-performance parts has brought a renaissance of research interest to this field. For instance, specialized FDM techniques have been developed to process high-performance thermoplastic materials, e.g., Polyetheretherketone (PEEK) [4] and fiber-reinforced polymer composites (FRPC)[5]. The modulus and strength of FDM fabricated FRPC can be improved up to one or two orders of magnitude than using polymers alone. Also, big area additive manufacturing (BAAM), a variant of the FDM process, has been developed to increase the build rate and extend the print volume for large-scale parts [6,7]. The strong demand for these emerging techniques has motivated researchers to gain deep insight into the underlying mechanisms of the FDM process.

One critical mechanism is the polymer melt flow during the extrusion and deposition, which underpins the FDM technique and its advanced variants. The behavior of melt flow directly affects the FDM process's producibility, repeatability, and reproducibility. A clear understanding of this mechanism will form the basis for further applications, e.g., nozzle design and in-process control. However, most existing research [8–18] investigates the melt flow indirectly, in which its influences on the performance of fabricated parts are studied through experiments. In other words, parts are fabricated with different melt flows by adjusting the process settings, e.g., printing velocity [8,9,17] and nozzle temperature [9,13], thereafter their properties are characterized. However, the above methods cannot provide sufficient information to guide researchers for more complicated scenarios, e.g., extrusion at varied velocities and extrusion for extreme conditions. In-process monitoring is an attractive approach for directly observing the ongoing phenomenon [19–22]. However, the limited accessibility makes the measurements prohibitively difficult, which is intangible to implement. Simulation-based methods provide a versatile solution to intuitively and rapidly understand the evolution of the melting and deposition process.

This review aims to summarize the recent progress on the melt flow simulations of FDM for polymers and their fiber-reinforced composites. Fig.1 illustrates the fundamentals of the FDM process. The printhead, which is the core component of an FDM printer, consists of a filament feeding mechanism and a hot-end. The feeding mechanism, made up of a stepper motor and a drive block, continuously supplies the raw material filament into the hot-end. The hot end is responsible for heating the filament to be melted and successfully extruded, then, the extruded molten polymer brings into contact with the substrate and follows the printhead to move layer by layer to form the part. The influence of the deformation of the filament on the printing process can be ignored in the feeding process. Therefore, the simulations of the FDM process mainly focus on the process from the filament entry into the hot end to deposition on the substrate. The melt flow simulations can be divided into two parts: the extrusion process through a nozzle and the deposition process above a print bed. The thermodynamic models of pure polymer in the nozzle of FDM with analytical and numerical methods are discussed first. Then, an overview of numerical research about the polymer melt flow in the deposition process of FDM is presented examining both single-strand and multi-strand deposition. In addition, the FDM process simulation of short and continuous fiber-reinforced composites is also explored due to its significantly different phenomena. Finally, the article is concluded with an insight into the outlook of the future direction in numerical simulation of the FDM process. This work will contribute to exploring the application prospect of FDM process simulation and guiding the future research direction.

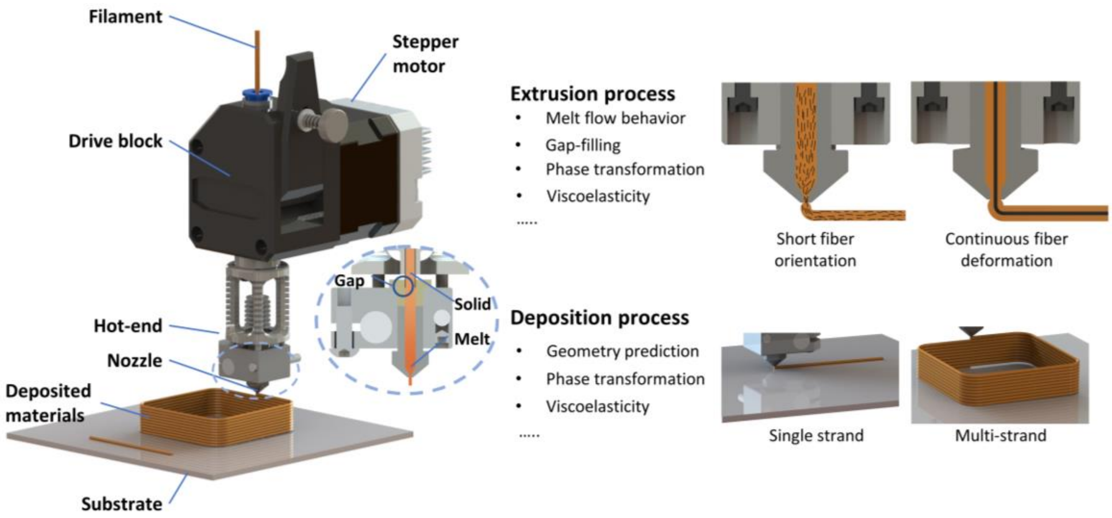

Fig.1. Melt flow simulations for polymers and their fiber reinforced composites in fused deposition modeling.

2. Intra-nozzle Process Simulations

2.1. Analytical models

Early attempts at intra-nozzle process simulations are mainly based on analytical melting models. Bellini et al. [23] are the first to utilize mathematic models as tools for investigating the melt flow phenomena and dynamics inside the liquefier. This research adopts a simplified non-isothermal flow in which the polymer in the hot-end is completely melted, and the temperature distribution is uniform and space-independent (Fig.2 (a)). The rheological behaviors of melted polymers, i.e., shear-thinning and temperature dependency, are described by the Power-law and Arrhenius models, respectively. The governing equations are based on the conservation law of fluid momentum and mass for calculating the pressure drop and evolution of flow rate. Meanwhile, the transfer function of the liquefier is established on the analogy of an amplifying circuit to predict the response of the flow field under different inputs, and its effectiveness is experimentally validated. The model is later applied as a part of a simulation system to support process optimization and real-time monitoring for feeding forces [24]. Phan et al. [25] further extend the model by considering the extensional viscosity effects using a modified Cogswell model [26] to investigate the pressure drop. The model's predictions on pressure drop have been compared with experimental measurements by adjusting the Trouton ratio, which is the ratio of extensional viscosity to shear viscosity and measures the strength of elasticity in the melt flow.

The above models are not valid for processes with high feed rates, in which the filament is not completely melted until the bottom of the liquefier. Thus, Osswald et al. [27] have proposed an analytical model, in which a melt film is modeled on the surface of the conical section, for incorporating the phase transformation of polymer from solid to melt states (Fig.2 (b)), and validated it with an in-house developed test setup. In later studies, Peng et al. [28] have established an analytical model to describe the flow profile inside the hot-end channel with assumptions of isothermal flow and Power-law fluid and applied Computer Tomography (CT) to scan the nozzle with a solidified pigment filament. It is found that the model prediction deviates from the measured velocity profile due to the oversimplification of the melt flow's non-uniform temperature distribution. In addition, a more advanced analytical model has been proposed for studying the deformation of the polymer during the FDM process [29]. They have adopted a modified continuum molecularly aware polymer model with flow-induced disentanglement and found that the polymer deformation is affected primarily by the deposition flow rather than the intra-nozzle flow. Also, the polymer deformation increases with the printing velocity.

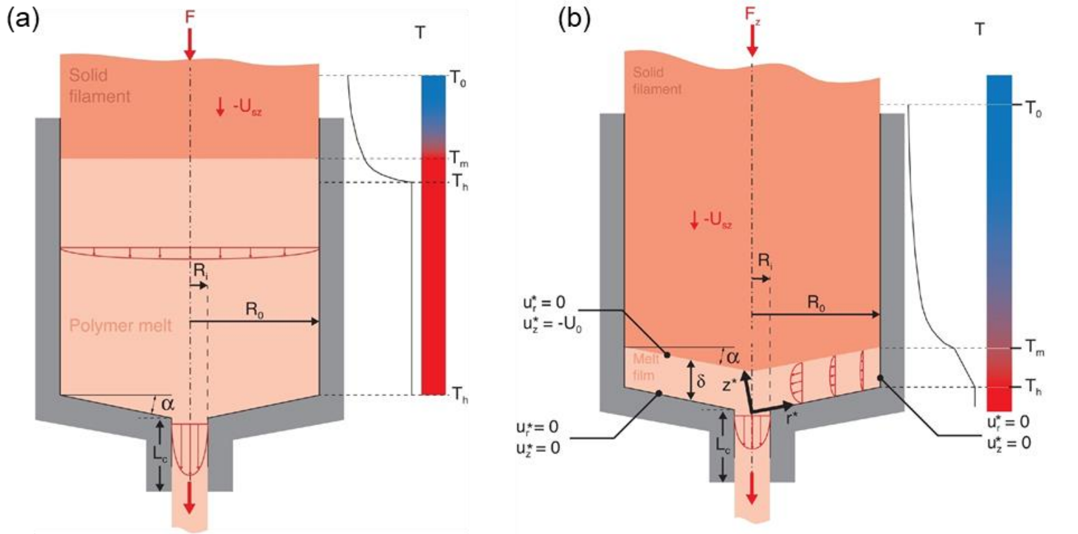

Fig.2. (a) Melting and flow model assumed [23]by Bellini et al. [23]; where T_0, T_m, T_h are initial temperature, melt temperature of polymer, and heating temperature from hot-end. The temperature distribution of polymer in the hot-end is uniform; (b) Improved model in which a small melt film on the surface of conical section plays a significant role in phase transformation. Reprinted with permission from reference [27], Copyright 2018, Elsevier.

As discussed in previous works [23–25,27–29], analytical models are often quick to solve, making these an attractive tool for real-time applications, e.g., process monitoring and control. However, these analytical models have been developed for predicting specific quantities of interest, e.g., pressure drop and flow rate, rather than a comprehensive prediction of all quantities. Also, the analytical models often idealize and simplify the physical process, leading to significant inaccuracies in simulating complex physical processes. Therefore, recent studies have used numerical models for investigating complex phenomena.

2.2. Numerical models

Although previous studies have investigated various numerical melting models, the following standard procedure can be summarized to construct computational fluid dynamics (CFD) models. The modeling process includes nozzle geometry modeling, fluid flow model selection, material property definition, boundary condition definition, and numerical methods selection. The selection of fluid flow models, i.e., laminar or turbulent flow models, depends on the Reynolds number. In a typical scenario, the outlet diameter of the nozzle, outlet velocity, and polymer density, are less than 1 mm, 120 mm/s, and 10 g/cm^3 , respectively. Thus, the Reynolds number is less than one and the fluid flow is laminar. In terms of material property definition, the basic thermophysical and rheological properties of materials that should be considered are density, viscosity, specific heat, thermal conductivity, melting enthalpy, and melting temperature. Afterward, boundary conditions, including the velocity at the inlet, atmospheric pressure at the outlet, wall temperature, and heat transfer conditions, need to be defined. Once these conditions are established, numerical methods such as the finite difference method, finite element method (FEM), and finite volume method (FVM) are used for solving the governing equations. These simulations are often performed within CFD software tools, including Fluent, Polyflow, OpenFOAM, COMSOL, and FLOW-3D [4,30–39].

Previous simulations have investigated the use of various constitutive models for thermoplastic melts. Table 1 summarizes typical thermophysical and rheological models. In terms of material density, temperature-dependent models have been studied [4,31,33,38], though most research treats the density as constant. Also, the impact of material compressibility on the density has been only considered in the study of Kattinger et al. [38]. Regarding the rheology behavior of polymer melts, most studies have utilized classical Generalized Newtonian Fluid (GNF) models [4,31–35,37–40], such as the Carreau-Yasuda, Power-Law, and Cross models, to describe the shear rate ($\dot{\gamma}$) dependent behavior of the viscosity. Meanwhile, Arrhenius [32,35,37,39,40] or Williams-Landel-Ferry (WLF) [4,33,38,41] models are often adopted for depicting the temperature dependence of viscosity. Meanwhile, some research has applied the viscoelastic model, e.g., Giesekus [30,41] and Phan-Thien-Tanner (PTT) [34] models, which consider the elastic effect and are more accurate yet complex, compared to traditional rheological models. For thermal properties, previous studies [31,32,34,38] have modeled the specific heat capacity as a function of temperature. Moreover, recent studies [33,38] have taken into account other complex material properties, e.g., the pressure-dependent glass transition temperature $T_{glass}(p)$, temperature-dependent melting enthalpy $h(T)$, and temperature-dependent thermal conductivity $\kappa(T)$,and temperature-dependent thermal radiation intensity $\dot{q}_{rad}(T)$.

Table 1 Summary of numerical melting models for the FDM process.

Author	Research application	Material	Parameters of the thermal flow model			Tools	Ref.
			Density	Viscosity	Thermal		
Shadvar et.al	Melt flow behavior	Acrylonitrile Butadiene Styrene (ABS)	Constant	$\mu(\dot{\gamma}, T)$ (Power-law& Arrhenius)	Constant	Fluent	[37]
Phan et.al	Melt flow behavior & viscoelastic model	Polylactide (PLA)	Constant	$\mu(\dot{\gamma})$(Carreau-Yasuda) /$\mu(\dot{\gamma}, \sigma)$(PTT)	$C_p(T)$, others are constant	Fluent/ Polyflow	[34]
Ufodike et.al	Melt flow behavior	ABS	Constant but differ in phases	$\mu(\dot{\gamma}, T)$ (Power-law& Arrhenius)	$C_p(T)$, others are constant	Fluent	[32]
Kattinger et.al	Melt flow behavior	Polystyrene (PS)	$\rho(p, T)$	$\mu(\dot{\gamma}, T)$ (Cross&WLF)	$C_p(T)$, $\kappa(T)$ $h(T)$,$T_{glass}(p)$	OpenFOAM	[38]
Schuller et.al	Melt flow behavior	Polycarbonate (PC)	Constant	$\mu(\dot{\gamma}, \sigma)$ (Giesekus)	-	OpenFOAM	[30]
Serdeczny et.al	Melt flow behavior & geometric effect	ABS	Constant	$\mu(\dot{\gamma}, \sigma, T)$ (Giesekus& WLF)	Constant	OpenFOAM	[41]
Serdeczny et.al	Melt flow behavior & gap-filling	PLA	$\rho(T)$	$\mu(\dot{\gamma}, T)$ (Powe-law& WLF)	$\dot{q}_{rad}(T)$, others are constant	FLOW-3D	[33]
Marion et al.	Melt flow behavior & gap-filling	ABS	Constant	$\mu(\dot{\gamma}, T)$ (Carreau-Yasuda & Arrhenius)	Constant	Self-programming	[40]
Zhang et.al	Temperature distribution & change	PLA	$\rho(T)$	$\mu(\dot{\gamma})$ (Power-law)	$C_p(T)$, others are constant	Fluent	[31]
Idris et. al	Temperature setting	PLA	Constant	$\mu(\dot{\gamma}, T)$ (Power-law& Arrhenius)	Constant	Fluent	[39]
Papon et.al	Nozzle outlet design	PLA	Constant	Constant	Constant	Fluent	[36]
Go et.al	Nozzle design &velocity bound setting	-	Constant	$\mu(\dot{\gamma}, T)$ (Power-law& Arrhenius)	Constant	COMSOL	[35]
Wang et.al	Temperature & velocity bound setting	Polyetheretherketone (PEEK)	Constant	$\mu(\dot{\gamma}, T)$ (Cross-WLF)	Constant	Fluent	[4]

Although the material models chosen in previous studies are different, some similarities can be found among the results obtained [4,30–39]. Firstly, most studies have found that the pressure drop changes mainly occurred in the conical part of the nozzle, and the magnitude of the pressure drop is proportional to the polymer feed rate (Fig.3 (a)). Secondly, the temperature distribution of the molten polymer, and consequently the solid-melt interface, in the hot-end channel is a smooth cone-like surface with the tip pointing downward (Fig.3 (b)). The position of the interface moves toward the nozzle outlet with an increase in the feed rate. Thus, the polymer filament is prone to clog the nozzle at a high feed rate due to insufficient melting. In addition, the recirculation vortex is found between the liquefier wall and the filament that just gets molten, as depicted in Fig.3. (b). Some studies have speculated that this recirculation vortex is formed by the drag flow generated by the moving filament that acts to counteract overflow [32–34]. In terms of heat transfer conditions, some studies [33,34,42] have found that the increase in the wall heat transfer coefficient and heating temperature accelerates the melting of the polymer.

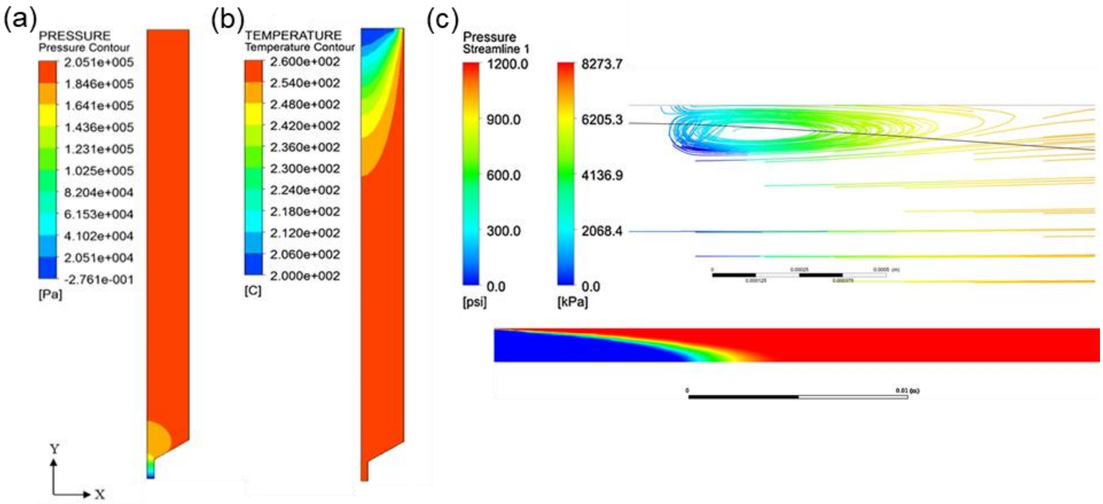

Fig.3. Pressure (a) and temperature (b) distribution of the ABS extrusion. Reprinted with permission from reference [37], Copyright 2019, Springer. (c) Above: the distribution of the pressure drop in the vortex region; below: the region of solidification (blue) and melting (red). Reprinted with permission from reference [34], Copyright 2020, Elsevier.

The aforementioned simulations consider the polymer melt as GNF, which neglects the elastic memory effect of the polymer. Thus, applying the viscoelastic model to examine the elastic effect on polymer during the FDM process is of great interest. Tomás Schuller et al. [30] have simplified the fluid domain from 3D to 2D (two-dimensional) according to the axial symmetry of the FDM nozzle pipeline, which significantly reduces computational time and cost. The research has assumed the flow in the nozzle as isothermal flow and adopted the Giesekus model to characterize the polymer viscoelasticity. It is revealed that whether the tensile flow is stronger than the shear flow at a certain point in the fluid domain depends on the positive or negative normal stress difference at that point. There is a large interaction force between the polymer melt and the nozzle's conical part, which changes the unidirectional stress state of the melt and its flow direction, enlarge the normal stress difference, and strengthen the elastic effect. The shear elastic stress is dominant in the backflow in the solid filament that enters the print-core and the liquefier wall. The study has also predicted the location of the recirculation vortex that occurred. Serdeczny et al. [41] have improved this model to reflect the actual non-isothermal flow in the FDM process by employing the WLF model for depicting the temperature dependency of the rheological parameters in the Giesekus model. In contrast to the commonly used GNF model, the use of this viscoelastic model can significantly improve the prediction accuracy of the pressure drop for printing with high feed rates.

In recent studies, the filling process for the gap between the polymer filament and the inner wall of the hot-end channel has been investigated. Serdeczny et al. [33] and Marion et al. [40] have improved the geometric model and applied a multiphase model to characterize the gap-filling process. Fig.4 (a) shows the comparison between models without and with the gap-filling process, which indicates more time is required to reach the steady state to form a stable backflow region due to the gap-filling process. However, it is found that when the feed rate is higher than a certain limit, the position of the backflow region in the new model will not remain stable. Otherwise, there is no difference between the two models. Researchers have speculated that this might be related to overflowing [33]. At high feed rates, the radial heat conduction will not be enough to melt the polymer in time, and the filament may be directly pushed down in the channel. When the filament contacts the conical section of the nozzle, the pressure applied to the polymer becomes larger. Then, the backflow is generated to fill the gap upward and increase the contact area between the filament and liquefier wall, which increases the melt temperature and decreases the viscosity and overall pressure. Such fluctuation of the gap-filling level repeats while the filament is feeding. Meanwhile, Ye et al. [22] have observed these phenomena using a transparent nozzle. In addition, it is found that the gap-filling level fluctuation occurs when the feed rate is beyond a threshold. A too-high feed rate will cause overflow from the hot-end and clog the print head. Meanwhile, the change of the feeding force under high feed rates has been studied by Serdeczny et al. [33], as depicted in Fig.4. (b), which has revealed that considering the gap-filling process and a proper thermal contact condition can improve the simulation accuracy.

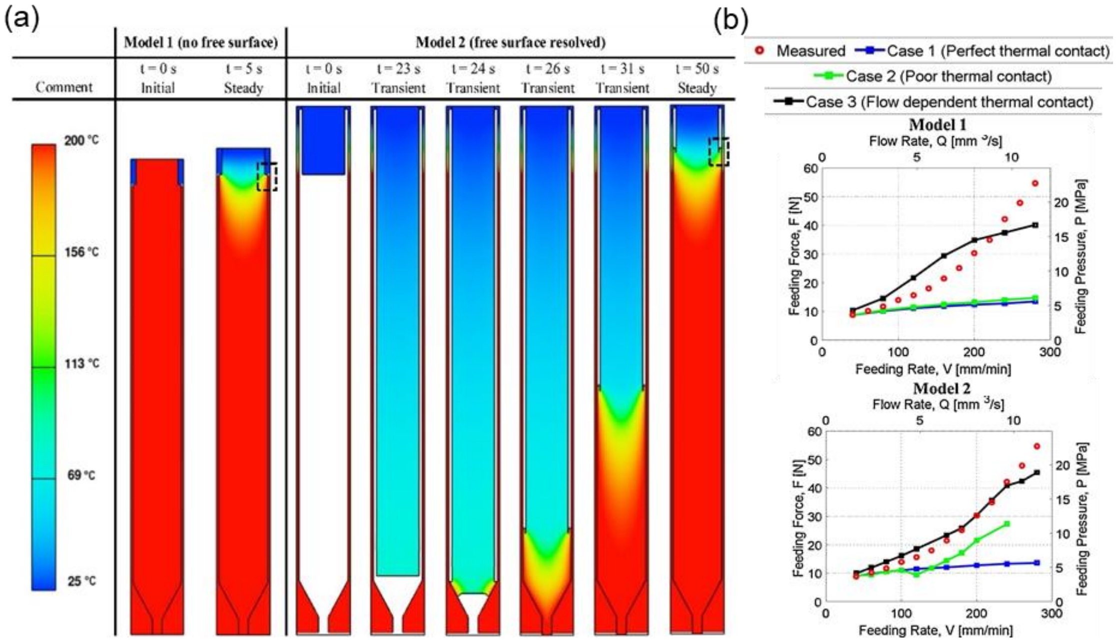

Fig.4 (a) Comparison of models without (Model 1) and with (Model 2) gap-filling process; and (b) the change of the feeding force under different models and thermal contact conditions.

Reprinted with permission from reference [33], Copyright 2020, Elsevier.

2.3. Applications of numerical method in FDM

Through the above numerical simulations, the influence of the hot-end's material, geometry, and heat transfer conditions on printing performance, such as maximum printing velocity and heating temperature, can be predicted. Thus, there are some potential applications in engineering design for FDM numerical simulation, such as optimizing the parameters for the printing process, planning the printing path, or assisting with the print head design [31,35,36,39,43]. For example, Idris et al. [39] have studied the solid-liquid distribution of the polymer in the liquefier to determine the heating temperature of the printer hot-end.

As shown in Fig. 5, some studies have determined the range of the feed rate according to whether the polymer is melted sufficiently before the nozzle outlet, which ensures fluent extrusion for the polymer [31,35]. Moreover, Comminal et al. [43] have concluded the characters of deposition at the corner and applied it in motion planning by numerical simulations.

In terms of print head design, numerical simulation is generally applied for verifying or comparing its printing performance. For instance, Papon et al. [36] have investigated the influence of different shapes of the nozzle outlet on printing performance by comparing pressure drop at the same feed rate. Go et al. [34] have used numerical simulations to verify the designed liquefier by simulating whether the polymer could be extruded smoothly. In addition, the numerical model has been persistently improved for investigating the change of feeding force with feed rate increasing [33,38,41], which is one of the important bases for print head design under various printing requirements, e.g., FDM rapid printing, conformal printing, printing for high-performance materials (e.g., PEEK) or soft materials (e.g., TPU).

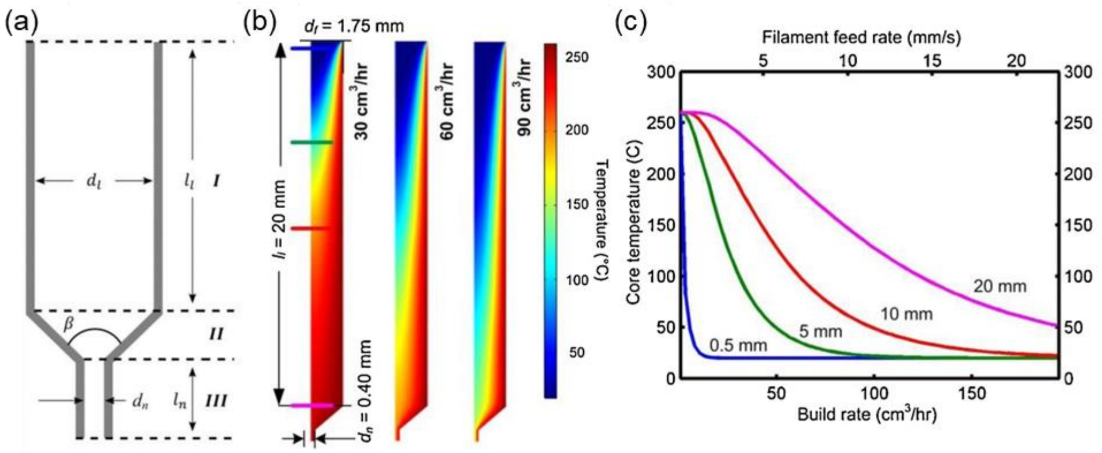

Fig. 5. A representative liquefier design case: First step：(a) design dimensions of liquefier; Second step：numerical simulation to determine the process parameters, (b) simulate the temperature distribution within the hot-end channel under different feed rate to ensure polymer melt sufficiently and easily extruded, (c) polymer temperature versus feed rate at noted distances in (b) to determine the range of feed rate. Reprinted with permission from reference [35], Copyright 2017, Elsevier.

3. Deposition Process Simulations

In the FDM process, the polymer melt is extruded through the hot-end and then deposited onto the platform to form parts layer by layer. The phase transformation of the polymer melt flow within the deposition process is a decisive factor that affects the deposition quality. Modeling such a process is a nontrivial task since it includes the forming of strands when the melt leaves from the nozzle and the partial re-melting to re-solidifying of existing strands near the strands being extruded. In addition, the deposition process simulation is a multi-phase problem with high computational costs, which involves the time-dependent phase change and the intricate interplay between different phases. The multi-phase model should be able to capture the evolution of the interface between air and polymer melt, i.e., the forming process of strands. Furthermore, previous studies [44–47] have found the shape of the extruded strand directly affects the performance of printed parts, e.g., surface roughness and porosity. Hence, recent studies have extensively investigated the use of multi-phase models for predicting the geometry of the strands. The rest of this section discusses the modeling of the two consecutive processes during the deposition. One is the single strand deposition, i.e., the strand-forming process when the melt leaves from the nozzle; another is multi-strand deposition corresponding to the re-solidification of existing strands near the strand being extruded.

3.1. Single strand deposition

Single-strand deposition means that polymer melt extrudes from the FDM nozzle to form a single bead on the print bed, as illustrated in Fig.6 (a). Numerical models with various complexities and accuracies have been developed, including models based on Newtonian [48] or non-Newtonian fluids [49,50], including isothermal [48,51–54] or non-isothermal flows [41,42]. For non-Newtonian fluid assumption, the Cross-WLF or Cross model [49,50], has been adopted. Meanwhile, material thermal parameters and heat transfer conditions [49,50], e.g., specific heat capacity, phase transition temperature, and wall heat transfer coefficient, have been considered for non-isothermal flow. It is found that the shear rate, temperature-dependent viscosity, and heat transfer conditions have a significant impact on improving simulation accuracy [50]. Meanwhile, the effects of surface tension and buoyancy on extrusion deposition have also been considered in previous works [49,52].

In the studies above, the influences of key factors, e.g., normalized printing head velocity V/U (extrusion volumetric flux U and printing head velocity V) and the normalized gap height g/D (nozzle position g above the substrate and the nozzle diameter D), on the cross-sectional profile of the strand have been studied [48,49,52–54]. The results show that the thickness of the strand increases with the increase of g/D, while curling phenomena [46] (Fig.6 (b)) can be observed if the normalized gap height g/D exceeds a threshold value. In addition, at the same g/D, with the increase of V/U, the ratio of thickness to the width of the strand and printing force will decrease. The simulation results match well with the experimental measurement at a low V/U and g/D [53]. Meanwhile, regarding the levelness of the strand, the simulation results deviate from the experimental measurements under the fluctuating feeding force. This is caused by the neglect of the viscoelastic effect within the model [52]. Furthermore, previous studies have also simulated the deposition process of core-shell polymer manufacturing [54], which is a variant of FDM that processes two polymers with distinct glass transition temperatures. It has been found that a good packing effect and a high-volume fraction of the core can be achieved by using large V/U, g/D, and inner nozzle diameter.

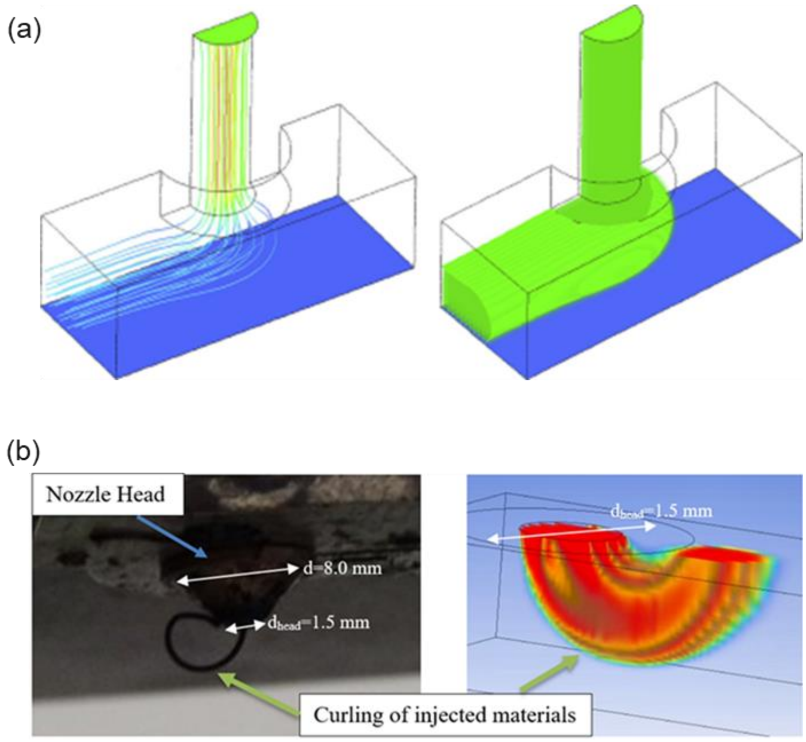

Fig.6. (a) An example of simulation for the deposition process of the single strand. Reprinted with permission from reference [48], Copyright 2018, Elsevier. (b) Curling phenomena observed in the experiments and numerical models. Reprinted with permission from reference

[49], Copyright 2021, Elsevier.

3.2. Multi-strand Deposition

In multi-strand deposition simulations, previous studies have focused on predicting the interface between strands, which is critical to the geometry and mechanical properties of the final part. There have been a few existing methods for modeling and simulating the multi-strand deposition. The applied methods can be divided into three types according to the thermal condition and material constitutive models.

In Method 1, an isothermal flow assumption is made, the previously deposited and solidified material are treated as rigid bodies, and the last strand is deposited at the new substrate combined with previous solid strands and substrate [55] (Fig. 7 (a)). Method 2 only considers the non-isothermal assumption and assumes the interface between strands will change through a partial re-melting and re-solidification process [56,57] (Fig. 7 (b)). Based on Method 2, Method 3 employs the viscoelastic model [58,59] in numerical analysis and investigates the influence of viscoelasticity on the deformation between the strands [60]. It has been found that compared with the non-Newtonian viscous fluid model, there are obvious differences in extruding diameter, layer thickness, strand profile, and shape recovery over time (Fig. 7(c-d)). In other words, with the improvement of the model by these three methods, the prediction accuracy of multi-layer or multi-strand deposition will be gradually improved.

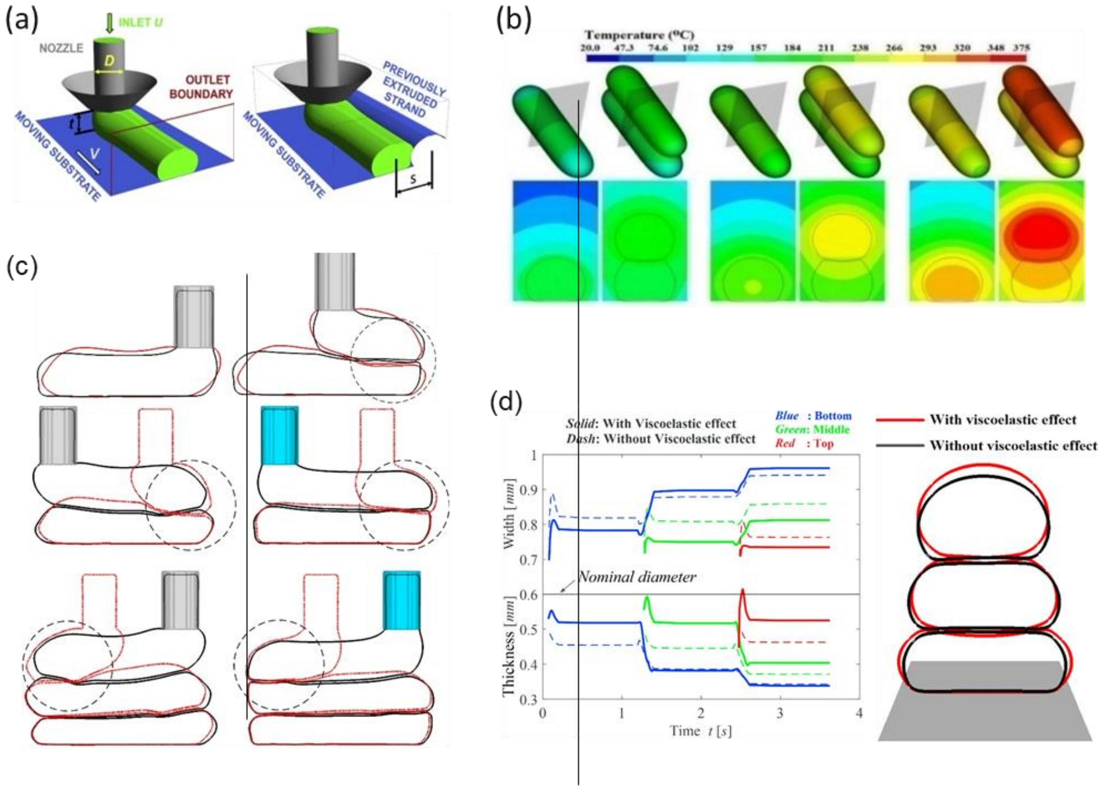

Fig. 7. (a) Interface between strands only determined by the previous strand surface. Reprinted with permission from reference [55], Copyright 2019, Elsevier. (b) The interface between strands changes with the reheating of the previous strand. Reprinted with permission from reference [56], Copyright 2017, Emerald. (c) The interface changes during the deposition process from the simulations with viscoelastic effect (black) and without viscoelastic effect (red); and (d) thickness and width of each layer versus time from simulations with viscoelastic effect (solid line) and without viscoelastic effect (dash line). Reprinted with permission from reference [60], Copyright 2018, Elsevier.

4. Process Simulations for Fiber-Reinforced Polymer Composites

FDM for FRPC is an emerging technique to fabricate lightweight but strong polymer composites in which fibers are utilized as the reinforced phase. Typical fiber types include carbon, glass, and Kevlar fibers. These fibers are either in short or continuous forms corresponding to two different processes. For short fibers, their polymer composite filaments can be directly used on commercial FDM machines without significant changes. However, the weight contents of short fiber in composites are often limited due to the reduced fracture strain. For continuous fibers, a co-extrusion strategy is often adopted to impregnate the fiber bundles with molten polymers [61]. These fibers form continuous load paths within fabricated composites, which possess one or two magnitudes higher mechanical properties than short-fiber reinforced composites. Since fibers are highly anisotropic materials, the alignment and orientation of fibers are critical to the mechanical properties of fabricated parts. In addition, other characteristics, such as the interface bonding properties, play an important role in it. Therefore, investigating the material flow and its interactions with fibers during the extrusion and deposition processes through simulations will be helpful for refining the FDM process for FRPC.

4.1. Process simulations for short fiber-reinforced composites

The melt flow simulation of short fiber composites is a fluid-structure coupling problem. In this problem, the fiber and molten polymer are considered as the solid and fluid phases, respectively. These two phases interact and influence each other. Accurate modeling of these complex interactions is one of the main challenges for process simulation. Table 2 summarizes details of previous studies on process simulations for short fiber-reinforced composites. The simulations based on CFD methods, such as FVM [62,63], FEM, and particle projection method, are often used for simulating the flow field. Moreover, the approaches for modeling fibers could be divided into three types. Method 1 models the fibers as rigid rods with an aspect ratio far greater than 1 [64–75]. Method 2 discretizes the short fibers into several rigidly connected small spheres or particles in the flow field [62,76]. Method 3 is to equivalent the mix of the fiber and polymer melt as pure fluid [77] and applies the moving particle semi-implicit (MPS) method to discretize the fluid into particles, in which the effect of fibers in the equivalent fluid is reflected in the viscosity model. In addition, this method has been validated by the experiment in predicting the cross-sectional profile of the deposited strand [77].

Table 2 Summary of numerical simulations for short fiber-reinforced composites in the FDM process.

Author	Research application	CFD method	Fibers model	Degree of coupling	Isothermal or Non-isothermal	Ref.
Yang et.al	Fracture	FVM	-	-	Isothermal	[63]
Imaeda et.al	Deposition	MPS	-	-	Non-isothermal	[77]
Smith et.al	Fiber orientation	FEM	Orientation tensor	Weak	Isothermal	[66–70]
				Full		[64,65,71,75]
Bertevas et.al	Fiber orientation	SPH	Orientation tensor	Full	Isothermal	[72]
					Non-isothermal	[73,74]
Yang et.al	Fiber orientation & nozzle clogging	SPH	DEM	Full	Isothermal	[76]
		FVM				[62]

Method 1 considers the fibers as rigid rods based on the Folgar-Tucker orientation tensor evaluation model [78], in which the aspect ratio and volume fraction of fibers are considered. With this method, the orientation of fibers in melt flow under the prescribed fluid velocity can be simulated [64–75]. In addition, the relationship between fibers and melt flow can be modeled as (i) weak coupling [66–70] or (ii) full coupling [64,65,71–75]. Specifically, the weak coupling model neglects the presence of fibers in the computation of melt flow kinematics. In the simulation, conservation equations of pure polymer melt flow are solved, then the velocity distribution is substituted into the orientation tensor evaluation model to get the fiber orientation state. This model is developed for studying the orientation of short fibers [66]. It is found that the fiber orientation tends to align along the direction of polymer melt flow, but the nozzle die swells hinder this trend. In addition, studies on BAAM have revealed that the planar extrudate swell, different polymer constitutive models, and screw swirling also have a direct impact on fiber orientation during the deposition process [67–70]. In contrast, the full coupling model considers the influence of fibers on the polymer melt flow, where the fiber orientation tensor is coupled into the momentum equation and energy equation in the form of stress (if a non-isothermal flow is assumed). Smith et al. [64] have developed a full coupling model with FEM [65,71] and found that the average value of fiber length distribution has a significant effect on the mechanical properties of the extruded strand [62]. Bertevas et al. [72] have established a full coupling model through the smoothed-particle hydrodynamics (SPH) method, a particle projection method, which discretizes the fluid domain into a series of particles for solving complex fluid problems [70]. Due to its computational rapidity distinguished from other numerical methods (such as FVM) for the CFD model, it is affordable to apply the non-isothermal conditions in the later simulation [73,74]. Research has found that the degree of fiber alignment on the surface of the deposited strand is better than that in the interior. This effect will become more pronounced with the increase of fiber concentration and the ratio of feed rate u to printing head velocity V [72]. The effect of the thermal conductivity of fibers has been revealed to enhance the fiber alignment along the deposition direction on the top half of the strand but weaken the fiber alignment on the bottom half of the strand. Meanwhile, it has been also found that the extrusion and deposition of the current layer will randomize the fiber orientation within the previously deposited layer. This effect can be aggravated by the increase of fiber concentration and fiber aspect ratio [73,74].

Method 2, called the discrete phase model (DEM), discretizes the short fibers as several rigidly connected particles in the polymer flow (Fig.8 (a)). In contrast to other methods, DEM considers the deformation of the fibers. This method has been used to investigate the fiber alignment and clogging during the extrusion in the studies by Yang et al. [62,76], in which the SPH and FVM are applied to simulate the flow field. Moreover, the prediction of this method has been validated by CT images (Fig.8 (b). Their studies have found that in the cone section of the nozzle, the fiber orientation tends to be parallel to the tapered wall, and the continued downward flow of the fibers causes cross-links. The longer the fibers are, the greater the possibility of cross-linking is. The cross-linking of the fibers results in a large pressure drop and even clogs the nozzle. One possible solution is to install a cone sleeve in the cone section of the nozzle, as illustrated in Fig.8 (c). Due to the cone sleeve, the reduction of the contact force between fibers near the outlet has been found in the simulation, which contributes to restrain the fiber cross-linking and nozzle clogging.

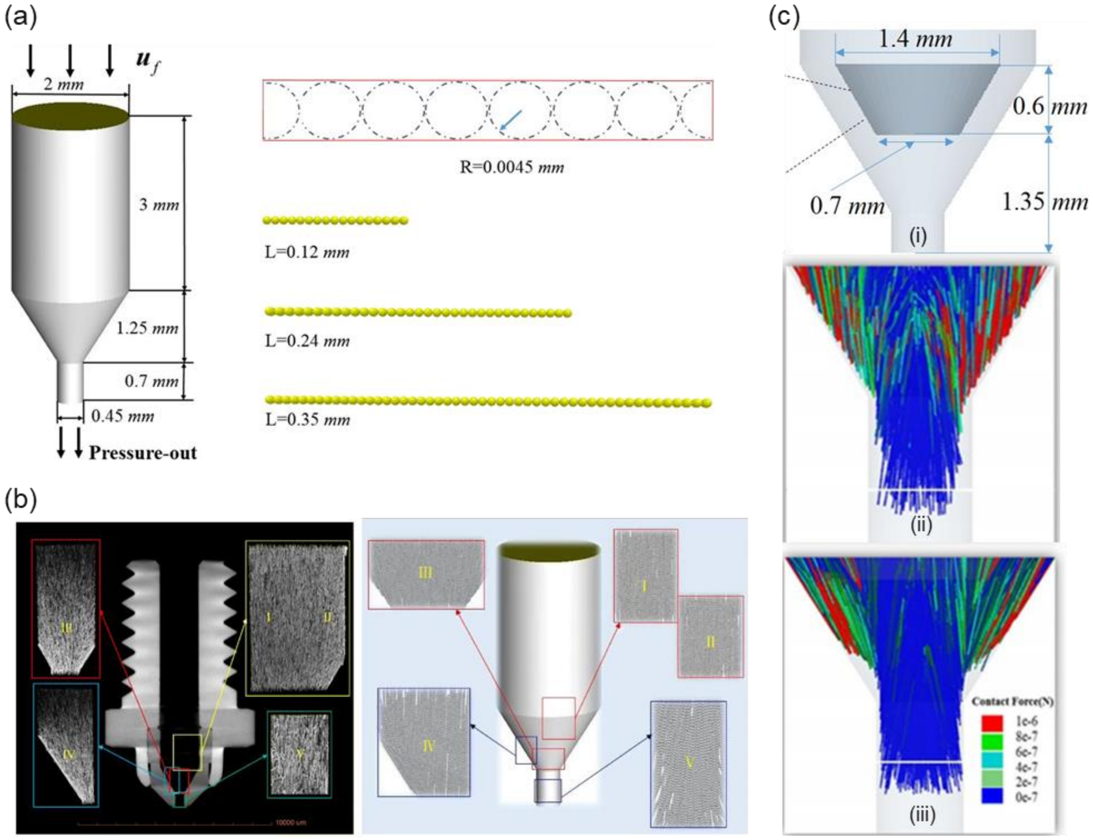

Fig.8. (a) Modeling of fiber and nozzle, where fibers are constituted of discrete DEM particles. (b) Fiber distribution in five regions: CT images (left) and numerical results (right); (c) Sketch of the cone sleeve (i) and distribution of DEM particles colored by their contact forces for origin nozzle (ii) or using cone sleeve (iii). Reprinted with permission from reference [62], Copyright 2021, Springer.

4.2. Process for continuous fiber-reinforced composite

As shown in Fig. 9, FDM for continuous fiber-reinforced composites (CFRP) can process both dry and pre-impregnated fiber bundles consisting of hundreds to thousands of continuous fibers. The critical difference is the existence of an in-situ impregnation process during extrusion, which significantly influences the mechanical properties of fabricated composites [79].

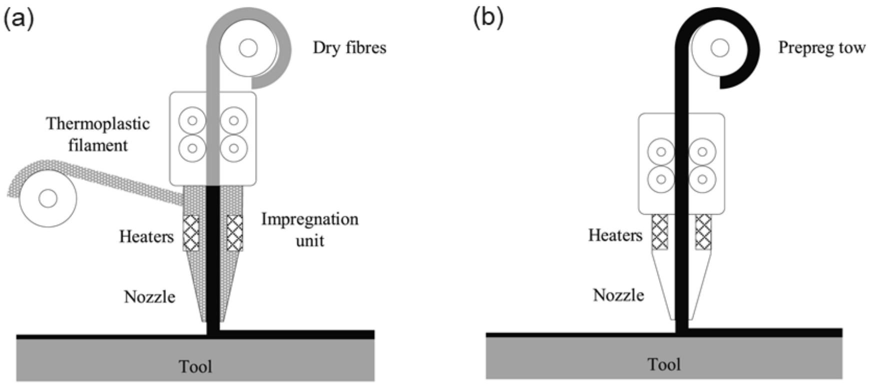

Fig. 9. Two typical FDM processes for CFRP: (a) in-situ impregnation and (b) pre-impregnation. Reprinted with permission from reference [79], Copyright 2021, Elsevier.

There are limited studies on the simulating continuous fiber-reinforced thermoplastic melt. In these studies, the fiber tow is often considered as a rigid sliding surface. Under this assumption, Han et al. [80] have used a numerical method for solving the isothermal Newtonian fluid model to calculate the pressure on the fiber to verify the feasibility of nozzle designs. Albrecht et al. [81] have proposed a computational fluid dynamics model with the non-isothermal viscosity model (Cross-Arrhenius) and viscoelastic model (K-BKZ), to assist the design for the geometry of the hot-end. The velocity and pressure drop profiles shown in Fig. 10 demonstrate the superiority of the modified hot-end design with fewer vortexes, residence times, and lower inlet pressure drops. In addition, the dimensions of the hot-end, i.e., length and outlet diameter, has been optimized using design objectives including the pressure drop, die swell ratio, and shear stress.

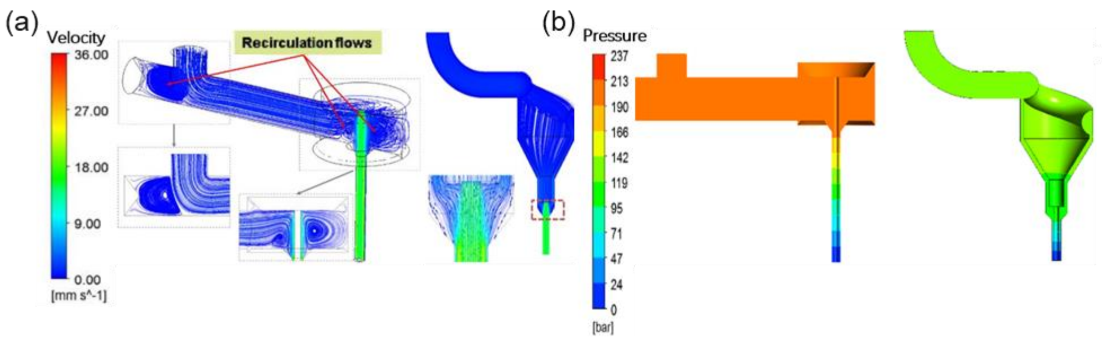

Fig. 10. (a) Streamlines within the 1st generation hot-end (left) and modified hot-end (right); and (b) pressure distribution within 1st generation hot-end (left) and modified hot-end (right). Reprinted with permission from reference [81], Copyright 2019, Sim-AM 2019.

In addition, Yang et al. [76] have adopted the DEM to study the deformation of long fiber tow within the melt flow by assuming the fiber tow as a line formed by a rigid connection of particles(Fig. 11 (a)). Meanwhile, the polymer fluid is considered as the Newtonian fluid under isothermal conditions. This study is the first to numerically investigate the extrusion and the deposition process for CFRP-FDM (Fig. 11 (b)), considering the fiber deformation. As shown in Fig. 11 (c), the shear stress concentration is conspicuous on the fiber at the nozzle outlet due to the bending. As an improvement, this study has pointed out that the 2D model can be extended to a 3D model in the future to study how continuous fiber is wrapped by the resin during the deposition process.

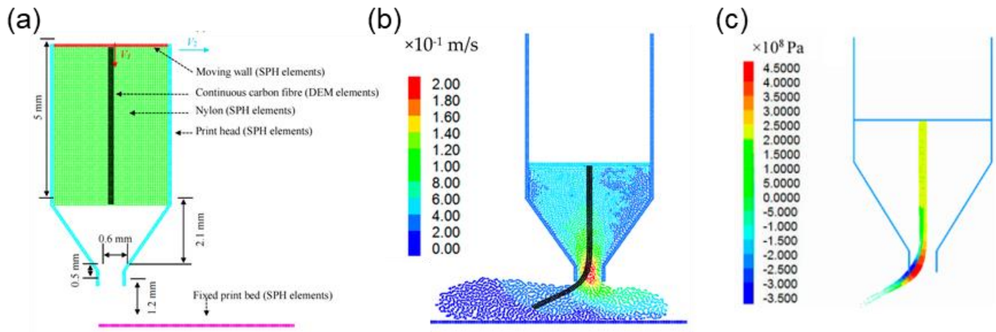

Fig. 11. (a) Schematic diagram of numerical modeling for CFRP-FDM. (b) Simulation result of CFRP-FDM extrusion and deposition process at t = 0.1 s. (c) Tensile stress distribution on the impregnated fiber tow at t = 0.1 s. Reprinted with permission from reference [76], Copyright 2017, MDPI.

The above studies model the fiber tow as a rigid sliding surface, or a thread constituted by rigidly connected spheres. However, this assumption is not valid for the in-situ impregnation-based CFRP-AM process, in which polymer melts penetrate into dry fiber bundles during the printing process. The degree of impregnation greatly affects the mechanical properties of continuous fiber-reinforced composites fabricated by FDM. Although related modeling methods have not been reported yet, the existing method for the conventional fiber impregnation process can be referred to. In general, there are two methods to model the fiber impregnation process. One is to treat the fiber tow as a moving porous medium [82–84]. This method ignores the local details of the fiber bundle and defines an anisotropic resistance to the fiber region. Another method considers fibers with a microscopic 2D model [85], as shown in Fig. 12, where fibers are assumed as rigid surfaces in a micro-scale CFD simulation, and it is combined with macro-scale CFD simulation to investigate the fiber impregnation process. Meanwhile, the pressure and velocity distribution from the macro-scale model are coupled with the micro-scale model. Consequently, the fiber impregnation in the FDM process of dry fiber co-extrusion can be thoroughly studied through the methods above [82–85]. However, these methods [82–85] fail to consider the impact of fiber deformation under the force from the fluid. Thus, new modeling methods are desired to be developed to explain the phenomenon of fiber deformation and simulate the complete printing process for CRRP.

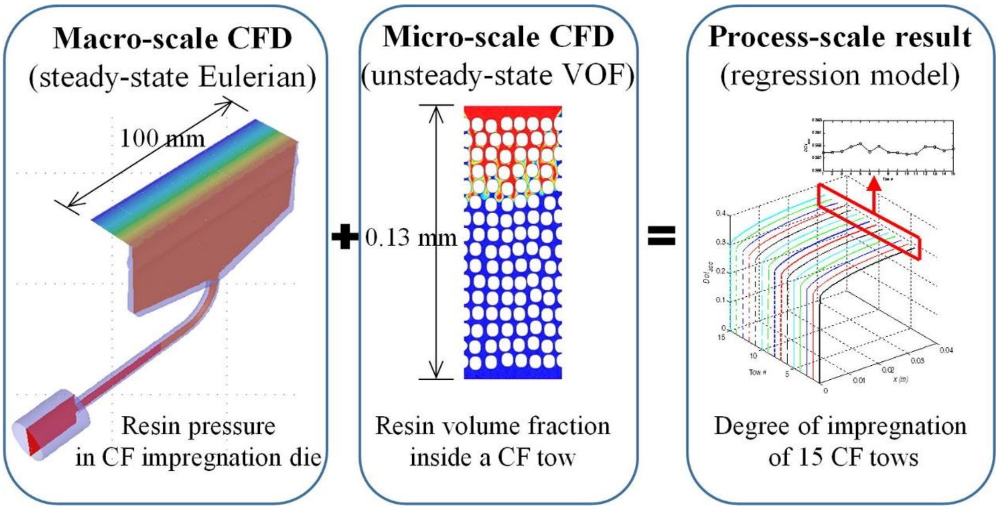

Fig. 12. Frame diagram of numerical simulation for fiber impregnation. Reprinted with permission from reference [85], Copyright 2021, Elsevier.

5. Conclusion

This study provides a comprehensive review of recent advances in melt flow simulations of the FDM process for polymers and their composites. Analytical and numerical methods for modeling the extrusion and deposition processes are summarized. Also, it outlines and discusses the process simulation for fiber composites which is an emerging research field. Finally, the following challenges are identified for inspiring future research:

a) Although various non-isothermal, nonlinear material properties have been thoroughly considered in current research, further research is needed to deeply understand the effects of polymer viscoelasticity on FDM process simulation and account for phenomena such as retracting and restarting.

b) Recent evidence suggests that the gap between the filament and the hot-end makes considerable impacts in the extrusion process of FDM. However, simulations and experiments still differ in their results due to the omission of the curvature of the filament.

c) For the FDM numerical simulation research of fiber-reinforced composites, in order to simulate the whole deposition process and spatial distribution of fiber orientation, it is urgent to transition from a 2D model to a 3D model, in which characterizing the fiber interaction and decreasing the computation cost are possible directions.

d) In the perspective of FDM simulation for continuous fiber-reinforced composites, there is a vast and undeniable research gap in modeling the fiber and its interaction with resin in the flow field. This includes studying factors such as fiber deformation and fiber impregnation.

e) There is a need to explore additional applications of simulation models. For instance, these simulations can play a critical role in the optimization of the print head structure and printing process parameters for emerging FDM processes, e.g., for fiber-reinforced composites.

Nomenclature

Stated material properties and printing parameters:

μ	Dynamic viscosity
$\dot{\gamma}$	Shear rate
ρ	Density
C_p	Specific heat capacity
h	Melting enthalpy
κ	Thermal conductivity
T_{glass}	Glass transition temperature
$\dot{q}_{rad}$	Thermal radiation intensity
g	Gap height (nozzle position above the substrate)
D	Nozzle diameter
g/D	Normalized gap height
u	Feed rate (the velocity of filament entering the hot-end)
U	Extrusion volumetric flux (average velocity inside the nozzle)
V	Printing head velocity (printing velocity)
V/U	Normalized printing head velocity
T	Temperature
p	Pressure

Acknowledgments

X.Y. acknowledges the National Key Research and Development Program of China [Grant No.2021YFB1715400], National Natural Science Foundation of China [Grant No.52105261] and the Department of Education of Guangdong Province [No. 2022ZDZX3020].

Appendix

Governing equations

The general form of governing equations for non-isothermal, viscous, incompressible, non-Newtonian fluid flow are as follows:

$$\boldsymbol{\nabla} \cdot \boldsymbol{u} = 0 \tag{1.}$$

$$\rho \frac{D\boldsymbol{u}}{Dt} = -\boldsymbol{\nabla} p + \boldsymbol{\nabla} \cdot \bar{\bar{\boldsymbol{\tau}}} + \rho \boldsymbol{g} \tag{2.}$$

$$\rho C_p \frac{DT}{Dt} = k\boldsymbol{\nabla}^2 T + \bar{\bar{\boldsymbol{\tau}}} : \boldsymbol{\nabla u} \tag{3.}$$

Where $\boldsymbol{u}$ is the velocity vector; ρ is the fluid density; t is the time; p is the pressure; $\bar{\bar{\boldsymbol{\tau}}}$ is the constitutive stress tensor; g is the gravitational acceleration vector; C_p is the specific heat; T is the temperature; and k is the thermal conductivity of the polymer.

Constituted model

Generalized Newtonian Fluid (GNF) models mentioned above:

The constitutive stress tensor $\bar{\bar{\boldsymbol{\tau}}}$ in Eqs. (1)-(3) typically depends on the instantaneous strain rate for GNF models, expressed as:

$$\bar{\bar{\boldsymbol{\tau}}} = \eta \boldsymbol{D} \tag{4.}$$

Where $\boldsymbol{D}$ is the instantaneous strain rate, calculated as: $\boldsymbol{D} = \frac{1}{2}(\nabla \boldsymbol{u} + \nabla \boldsymbol{u}^T)$, and η is the shear viscosity, described by GNF models as follows:

Power-Law model

$$\eta(\dot{\gamma}) = k(\dot{\gamma})^{n-1} \tag{5.}$$

Where η is the shear viscosity, γ is the true shear rate, k is the material consistency, and n is the power law index.

Carreau-Yasuda model

$$\eta(\dot{\gamma}) = \eta_\infty + \left(\eta_o - \eta_\infty\right)[1 + (\lambda\dot{\gamma})^a]^{n-\frac{1}{a}} \tag{6.}$$

Where $\eta(\dot{\gamma})$, η_∞, η_o, λ, a, and n are the shear viscosity, infinite-shear viscosity, zero-shear viscosity, relaxation time, transition index, and power-law index.

Cross model

$$\eta(\dot{\gamma}) = \frac{\eta_o}{[1 + ((\eta_o/\tau^*)\dot{\gamma})^{1-n}]} \tag{7.}$$

Here $\eta(\dot{\gamma})$, η_o, are the shear viscosity, and zero-shear viscosity respectively, and τ^* is the critical shear stress at the transition from the Newtonian plateau, n is the power-law index.

Viscoelastic models mentioned above:

For the viscoelastic constitutive model, accounting for memory effects (indicating internal stress of the fluid depends not only on the current deformation rate but also on its past deformation history), the constitutive stress tensor $\boldsymbol{\tau_s}$ in Eqs. (1)-(3) is typically decomposed into two parts as:

$$\bar{\bar{\boldsymbol{\tau}}} = \boldsymbol{\tau_s} + \boldsymbol{\tau_p} \tag{8.}$$

where $\boldsymbol{\tau_s}$is commonly called the solvent stress contribution, and $\boldsymbol{\tau_p}$ is called the polymer stress contribution. The solvent stress contribution depends on the instantaneous strain rate $\boldsymbol{D}$ and is general modelled with newton's law, calculated as:$\boldsymbol{\tau_s} = \eta_s \boldsymbol{D}$; where η_s is the solvent viscosity contribution. And $\boldsymbol{\tau_p}$ the polymer stress contribution is modeled with viscoelastic models as follows:

Phan-Thien-Tanner (PTT) model [86,87]

$$\exp\left[\frac{\varepsilon\lambda}{\eta_p}\mathrm{tr}(\boldsymbol{\tau_p})\right]\boldsymbol{\tau_p} + \lambda\left[\left(1-\frac{\xi}{2}\right)\boldsymbol{\tau_p} + \frac{\xi}{2}\boldsymbol{\tau_p}\right] = 2\eta_p\boldsymbol{D} \tag{9.}$$

Where, ξ and ε are material parameters that control, respectively, the shear viscosity and elongational behavior, and λ, η_p are the relaxation time, and polymer viscosity contribution.

Giesekus model

$$\boldsymbol{\tau_p} + \lambda\overset{\nabla}{\boldsymbol{\tau}}_{\boldsymbol{pk}} + \alpha\frac{\lambda}{\eta_p}\boldsymbol{\tau_p}\cdot\boldsymbol{\tau_p}^T = 2\eta_p\boldsymbol{D} \tag{10.}$$

where λ, α, η_p are the relaxation time, mobility factor, and polymer viscosity contribution, respectively.

K-BKZ model [88]

$$\boldsymbol{\tau_p} = \frac{1}{1-\theta}\int_{-\infty}^{t}\sum_{k=1}^{N}\frac{a_k}{\lambda_k}\exp\left(-\frac{t-t'}{\lambda_k}\right)\left(\frac{\alpha}{(\alpha-3)+\beta I_{C^{-1}}+(1-\beta)I_C}\right)\left[\boldsymbol{C_t^{-1}}(\boldsymbol{t}') + \boldsymbol{\theta C_t}(\boldsymbol{t}')\right]dt' \tag{11.}$$

where a_k and λ_k are the relaxation modulus and relaxation time for mode k, N is the number of relaxation modes, t is the current time. α and β are non-linear material constants, θ is a scalar parameter that controls the ratio of the normal stress differences, I_C and $I_{C^{-1}}$ are the first invariants of the Cauchy-Green strain tensor $\boldsymbol{C_t}$ and its inverse $\boldsymbol{C_t^{-1}}$, the Finger strain tensor.

Time-Temperature Equivalence Principle mentioned above:

The temperature-dependent viscosity is often modeled as:

$$\eta(\dot{\gamma}, T) = H(T)\eta(\dot{\gamma}) \tag{12.}$$

Where $H(T)$ is the temperature shift factor that modifies the viscosity according to the polymer temperature, following the time-temperature equivalence principle as follows:

Arrhenius Equation

$$H(T) = \exp\left[\frac{E_a}{R}\left(\frac{1}{T} - \frac{1}{T_{\mathrm{ref}}}\right)\right] \tag{13.}$$

where T_{ref} is the reference temperature, E_a is the activation energy, and R is the gas constant.

William-Landel-Ferry (WLF) Equation

$$H(T) = \exp\left[-\frac{C_1(T - T_{ref})}{C_2 + (T - T_{ref})}\right] \qquad (14.)$$

where C_1 and C_2 are the fitting constants, T_{ref} is reference temperature.

References

[1] Al Rashid A, Khan SA, G. Al-Ghamdi S, Koç M. Additive manufacturing: Technology, applications, markets, and opportunities for the built environment. Autom Constr 2020;118. https://doi.org/10.1016/j.autcon.2020.103268.

[2] Hull, C.W. Apparatus and method for creating three-dimensional objects. Google Patents 1986.

[3] Preview TS. INTERNATIONAL STANDARD ISO / ASTM Additive manufacturing — General principles — Fundamentals and vocabulary 2021;2021.

[4] Wang P, Zou B, Xiao H, Ding S, Huang C. Effects of printing parameters of fused deposition modeling on mechanical properties, surface quality, and microstructure of PEEK. J Mater Process Technol 2019;271:62–74. https://doi.org/10.1016/j.jmatprotec.2019.03.016.

[5] Liu G, Xiong Y, Zhou L. Additive manufacturing of continuous fiber reinforced polymer composites: Design opportunities and novel applications. Composites Communications 2021;27:100907. https://doi.org/10.1016/j.coco.2021.100907.

[6] Duty CE, Kunc V, Compton B, Post B, Erdman D, Smith R, et al. Structure and mechanical behavior of Big Area Additive Manufacturing (BAAM) materials. Rapid Prototyp J 2017;23:181–9. https://doi.org/10.1108/RPJ-12-2015-0183.

[7] Cleeman J, Bogut A, Mangrolia B, Ripberger A, Kate K, Zou Q, et al. Scalable, flexible and resilient parallelization of fused filament fabrication: Breaking endemic tradeoffs in material extrusion additive manufacturing. Addit Manuf 2022;56:102926. https://doi.org/10.1016/j.addma.2022.102926.

[8] Rezaeian P, Ayatollahi MR, Nabavi-Kivi A, Mohammad Javad Razavi S. Effect of printing speed on tensile and fracture behavior of ABS specimens produced by fused deposition modeling. Eng Fract Mech 2022;266. https://doi.org/10.1016/j.engfracmech.2022.108393.

[9] Yin B, He Q, Ye L. Effects of deposition speed and extrusion temperature on fusion between filaments in single-layer polymer films printed with FFF. Advanced Industrial and Engineering Polymer Research 2021;4:270–6. https://doi.org/10.1016/j.aiepr.2021.07.002.

[10] Doshi M, Mahale A, Singh SK, Deshmukh S. Printing parameters and materials affecting mechanical properties of FDM-3D printed Parts: Perspective and prospects. Mater Today Proc, vol. 50, Elsevier Ltd; 2021, p. 2269–75. https://doi.org/10.1016/j.matpr.2021.10.003.

[11] Daguilh T, Yang M. A joule heating mechanism for high-speed fused filament fabrication Signature redacted. 2019.

[12] Khan S, Joshi K, Deshmukh S. A comprehensive review on effect of printing parameters on mechanical properties of FDM printed parts. Mater Today Proc, vol.

50, Elsevier Ltd; 2021, p. 2119–27. https://doi.org/10.1016/j.matpr.2021.09.433.

[13] Aliheidari N, Tripuraneni R, Ameli A, Nadimpalli S. Fracture resistance measurement of fused deposition modeling 3D printed polymers. Polym Test 2017;60:94–101. https://doi.org/10.1016/j.polymertesting.2017.03.016.

[14] Yu Z, Gao Y, Jiang J, Gu H, Lv S, Ni H, et al. Study on effects of FDM 3d printing parameters on mechanical properties of Polylactic Acid. IOP Conf Ser Mater Sci Eng, vol. 688, Institute of Physics Publishing; 2019. https://doi.org/10.1088/1757-899X/688/3/033026.

[15] Kesava YV, Kumar A, Subbiah DR. Experimental investigation and optimization of process parameters in FDM printed abs samples for UAV application. International Journal For Recent Developments in Science & Technology 2019;03:189–92.

[16] Yu Z, Gao Y, Jiang J, Gu H, Lv S, Ni H, et al. Study on effects of FDM 3d printing parameters on mechanical properties of Polylactic Acid. IOP Conf Ser Mater Sci Eng, vol. 688, Institute of Physics Publishing; 2019. https://doi.org/10.1088/1757-899X/688/3/033026.

[17] Pappas JM, Thakur AR, Leu MC, Dong X. A parametric study and characterization of additively manufactured continuous carbon fiber reinforced composites for high-speed 3D printing n.d. https://doi.org/10.1007/s00170-021-06723-1/Published.

[18] Nabavi-Kivi A, Ayatollahi MR, Rezaeian P, Razavi SMJ. Investigating the effect of printing speed and mode mixity on the fracture behavior of FDM-ABS specimens. Theoretical and Applied Fracture Mechanics 2022;118. https://doi.org/10.1016/j.tafmec.2021.103223.

[19] Coogan TJ, Kazmer DO. In-line rheological monitoring of fused deposition modeling. J Rheol (N Y N Y) 2019;63:141–55. https://doi.org/10.1122/1.5054648.

[20] Kazmer DO, Colon AR, Peterson AM, Kim SK. Concurrent characterization of compressibility and viscosity in extrusion-based additive manufacturing of acrylonitrile butadiene styrene with fault diagnoses. Addit Manuf 2021;46:102106. https://doi.org/10.1016/j.addma.2021.102106.

[21] Chen J, Smith DE. Filament rheological characterization for fused filament fabrication additive manufacturing: A low-cost approach. Addit Manuf 2021;47:102208. https://doi.org/10.1016/j.addma.2021.102208.

[22] Hong Y, Mrinal M, Phan HS, Tran VD, Liu X, Luo C. In-situ observation of the extrusion processes of Acrylonitrile Butadiene Styrene and Polylactic Acid for material extrusion additive manufacturing. Addit Manuf 2022;49. https://doi.org/10.1016/j.addma.2021.102507.

[23] Bellini A, Güçeri S, Bertoldi M. Liquefier dynamics in fused deposition. Journal of Manufacturing Science and Engineering, Transactions of the ASME 2004;126:237–46. https://doi.org/10.1115/1.1688377.

[24] Moretti M, Rossi A, Senin N. In-process simulation of the extrusion to support

optimisation and real-time monitoring in fused filament fabrication. Addit Manuf 2021;38. https://doi.org/10.1016/j.addma.2020.101817.
[25] Phan DD, Swain ZR, Mackay ME. Rheological and heat transfer effects in fused filament fabrication. J Rheol (N Y N Y) 2018;62:1097–107. https://doi.org/10.1122/1.5022982.
[26] Cogswell FN. Converging flow of polymer melts in extrusion dies. Polym Eng Sci 1972;12:64–73. https://doi.org/10.1002/PEN.760120111.
[27] Osswald TA, Puentes J, Kattinger J. Fused filament fabrication melting model. Addit Manuf 2018;22:51–9. https://doi.org/10.1016/j.addma.2018.04.030.
[28] Peng F, Vogt BD, Cakmak M. Complex flow and temperature history during melt extrusion in material extrusion additive manufacturing. Addit Manuf 2018;22:197–206. https://doi.org/10.1016/j.addma.2018.05.015.
[29] McIlroy C, Olmsted PD. Deformation of an amorphous polymer during the fused-filament-fabrication method for additive manufacturing. J Rheol (N Y N Y) 2017;61:379–97. https://doi.org/10.1122/1.4976839.
[30] Schuller T, Fanzio P, Galindo-Rosales FJ. Analysis of the importance of shear-induced elastic stresses in material extrusion. Addit Manuf 2022:102952. https://doi.org/10.1016/J.ADDMA.2022.102952.
[31] Zhang J, Vasiliauskaite E, de Kuyper A, de Schryver C, Vogeler F, Desplentere F, et al. Temperature analyses in fused filament fabrication: from filament entering the hot-end to the printed part. 3D Print Addit Manuf 2021. https://doi.org/10.1089/3dp.2020.0339.
[32] Ufodike CO, Nzebuka GC. Investigation of thermal evolution and fluid flow in the hot-end of a material extrusion 3D Printer using melting model. Addit Manuf 2022;49. https://doi.org/10.1016/j.addma.2021.102502.
[33] Serdeczny MP, Comminal R, Mollah MT, Pedersen DB, Spangenberg J. Numerical modeling of the polymer flow through the hot-end in filament-based material extrusion additive manufacturing. Addit Manuf 2020;36. https://doi.org/10.1016/j.addma.2020.101454.
[34] Phan DD, Horner JS, Swain ZR, Beris AN, Mackay ME. Computational fluid dynamics simulation of the melting process in the fused filament fabrication additive manufacturing technique. Addit Manuf 2020;33. https://doi.org/10.1016/j.addma.2020.101161.
[35] Go J, Schiffres SN, Stevens AG, Hart AJ. Rate limits of additive manufacturing by fused filament fabrication and guidelines for high-throughput system design. Addit Manuf 2017;16:1–11. https://doi.org/10.1016/j.addma.2017.03.007.
[36] Papon MEA, Haque A, Sharif MAR. Effect of nozzle geometry on Melt flow simulation and structural property of thermoplastic nanocomposites in Fused deposition modeling. 32nd Technical Conference of the American Society for Composites 2017,

vol. 3, DEStech Publications Inc.; 2017, p. 2167–82. https://doi.org/10.12783/asc2017/15339.
[37] Shadvar N, Foroozmehr E, Badrossamay M, Amouhadi I, Dindarloo AS. Computational analysis of the extrusion process of fused deposition modeling of acrylonitrile-butadiene-styrene n.d. https://doi.org/10.1007/s12289-019-01523-1/Published.
[38] Kattinger J, Ebinger T, Kurz R, Bonten C. Numerical simulation of the complex flow during material extrusion in fused filament fabrication. Addit Manuf 2022;49. https://doi.org/10.1016/j.addma.2021.102476.
[39] Idris M, Ismail S. Analysis on temperature setting for extruding polylactic acid using open-source3D printer. ARPN Journal of Engineering and Applied Sciences 2017;12:1348–53.
[40] Marion S, Sardo L, Joffre T, Pigeonneau F. First steps of the melting of an amorphous polymer through a hot-end of a material extrusion additive manufacturing. Addit Manuf 2023;65:103435. https://doi.org/10.1016/J.ADDMA.2023.103435.
[41] Serdeczny MP, Comminal R, Mollah MT, Pedersen DB, Spangenberg J. Viscoelastic simulation and optimisation of the polymer flow through the hot-end during filament-based material extrusion additive manufacturing. Virtual Phys Prototyp 2022;17:205–19. https://doi.org/10.1080/17452759.2022.2028522.
[42] Pigeonneau F, Xu D, Vincent M, Agassant JF. Heating and flow computations of an amorphous polymer in the liquefier of a material extrusion 3D printer. Addit Manuf 2020;32. https://doi.org/10.1016/j.addma.2019.101001.
[43] Comminal R, Serdeczny MP, Pedersen DB, Spangenberg J. Motion planning and numerical simulation of material deposition at corners in extrusion additive manufacturing. Addit Manuf 2019;29. https://doi.org/10.1016/j.addma.2019.06.005.
[44] Rodríguez JF, Thomas JP, Renaud JE. Mechanical behavior of acrylonitrile butadiene styrene fused deposition materials modeling. Rapid Prototyp J 2003;9:219–30. https://doi.org/10.1108/13552540310489604.
[45] Ahn D, Kweon JH, Kwon S, Song J, Lee S. Representation of surface roughness in fused deposition modeling. J Mater Process Technol 2009;209:5593–600. https://doi.org/10.1016/j.jmatprotec.2009.05.016.
[46] Ahn D, Kweon JH, Choi JH, Lee SH. Relation between surface roughness and overlap interval in fused deposition modeling. Adv Mat Res, vol. 264–265, 2011, p. 1625–30. https://doi.org/10.4028/www.scientific.net/AMR.264-265.1625.
[47] Li L, Sun Q, Bellehumeur C, Gu P. Composite modeling and analysis for fabrication of FDM prototypes with locally controlled properties. J Manuf Process 2002;4:129–41. https://doi.org/10.1016/S1526-6125(02)70139-4.
[48] Comminal R, Serdeczny MP, Pedersen DB, Spangenberg J. Numerical modeling of the strand deposition flow in extrusion-based additive manufacturing. Addit Manuf

2018;20:68–76. https://doi.org/10.1016/j.addma.2017.12.013.

[49] Jahandardoost M, Milani AS. Multiphysics modeling and experimental investigation of the deposition process in fused filament fabrication method, under high-viscosity and non-Newtonian material flow. J Mater Eng Perform 2021;30:6913–23. https://doi.org/10.1007/s11665-021-06061-z.

[50] Kim SK, Kazmer DO. Non-isothermal non-Newtonian three-dimensional flow simulation of fused filament fabrication. Addit Manuf 2022:102833. https://doi.org/10.1016/j.addma.2022.102833.

[51] Du J, Wei Z, Wang X, Wang J, Chen Z. An improved fused deposition modeling process for forming large-size thin-walled parts. J Mater Process Technol 2016;234:332–41. https://doi.org/10.1016/j.jmatprotec.2016.04.005.

[52] Gosset A, Barreiro-Villaverde D, Permuy JCB, Lema M, Ares-Pernas A, López MJA. Experimental and numerical investigation of the extrusion and deposition process of a poly(Lactic acid) strand with fused deposition modeling. Polymers (Basel) 2020;12:1–20. https://doi.org/10.3390/polym12122885.

[53] Serdeczny MP, Comminal R, Pedersen DB, Spangenberg J. Experimental validation of a numerical model for the strand shape in material extrusion additive manufacturing. Addit Manuf 2018;24:145–53. https://doi.org/10.1016/j.addma.2018.09.022.

[54] Narei H, Fatehifar M, Malt AH, Bissell J, Souri M, Nasr Esfahani M, et al. Numerical Simulation of a Core–Shell Polymer Strand in Material Extrusion Additive Manufacturing. Polymers (Basel) 2021;13:476. https://doi.org/10.3390/polym13030476.

[55] Serdeczny MP, Comminal R, Pedersen DB, Spangenberg J. Numerical simulations of the mesostructure formation in material extrusion additive manufacturing. Addit Manuf 2019;28:419–29. https://doi.org/10.1016/j.addma.2019.05.024.

[56] Xia H, Lu J, Dabiri S, Tryggvason G. Fully resolved numerical simulations of fused deposition modeling. Part I: fluid flow. Rapid Prototyp J 2018;24:463–76. https://doi.org/10.1108/RPJ-12-2016-0217.

[57] Unverdi SO, Tryggvason G. A front-tracking method for viscous, incompressible, multi-fluid flows. J Comput Phys 1992;100:25–37. https://doi.org/10.1016/0021-9991(92)90307-K.

[58] McIlroy C, Olmsted PD. Deformation of an amorphous polymer during the fused-filament-fabrication method for additive manufacturing. J Rheol (N Y N Y) 2017;61:379. https://doi.org/10.1122/1.4976839.

[59] McIlroy C, Olmsted PD. Disentanglement effects on welding behaviour of polymer melts during the fused-filament-fabrication method for additive manufacturing. Polymer (Guildf) 2017;123:376–91. https://doi.org/10.1016/J.POLYMER.2017.06.051.

[60] Xia H, Lu J, Tryggvason G. A numerical study of the effect of viscoelastic stresses in fused filament fabrication. Comput Methods Appl Mech Eng 2019;346:242–59. https://doi.org/10.1016/j.cma.2018.11.031.
[61] Parandoush P, Lin D. A review on additive manufacturing of polymer-fiber composites. Compos Struct 2017;182:36–53. https://doi.org/10.1016/J.COMPSTRUCT.2017.08.088.
[62] Zhang H, Zhang L, Zhang H, Wu J, An X, Yang D. Fibre bridging and nozzle clogging in 3D printing of discontinuous carbon fibre-reinforced polymer composites: coupled CFD-DEM modelling. International Journal of Advanced Manufacturing Technology 2021;117:3549–62. https://doi.org/10.1007/s00170-021-07913-7.
[63] Yang Z, Yang Z, Chen H, Yan W. 3D printing of short fiber reinforced composites via material extrusion: Fiber breakage. Addit Manuf 2022;58:103067. https://doi.org/10.1016/j.addma.2022.103067.
[64] Wang Z, Smith DE, Jack DA. A statistical homogenization approach for incorporating fiber aspect ratio distribution in large area polymer composite deposition additive manufacturing property predictions. Addit Manuf 2021;43:102006. https://doi.org/10.1016/j.addma.2021.102006.
[65] Wang Z, Smith DE. Finite element modelling of fully-coupled flow/fiber-orientation effects in polymer composite deposition additive manufacturing nozzle-extrudate flow. Compos B Eng 2021;219:108811. https://doi.org/10.1016/j.compositesb.2021.108811.
[66] Heller BP, Smith DE, Jack DA. Effects of extrudate swell and nozzle geometry on fiber orientation in Fused Filament Fabrication nozzle flow. Addit Manuf 2016;12:252–64. https://doi.org/10.1016/j.addma.2016.06.005.
[67] Wang Z, Smith DE. Rheology effects on predicted fiber orientation and elastic properties in large scale polymer composite additive manufacturing. Journal of Composites Science 2018;2:1–18. https://doi.org/10.3390/jcs2010010.
[68] Heller BP, Smith DE, Jack DA. Planar deposition flow modeling of fiber filled composites in large area additive manufacturing. Addit Manuf 2019;25:227–38. https://doi.org/10.1016/j.addma.2018.10.031.
[69] Russell T, Heller B, Jack DA, Smith DE. Prediction of the fiber orientation state and the resulting structural and thermal properties of fiber reinforced additive manufactured composites fabricated using the big area additive manufacturing process. Journal of Composites Science 2018;2. https://doi.org/10.3390/jcs2020026.
[70] Wang Z, Smith DE. Numerical analysis of screw swirling effects on fiber orientation in large area additive manufacturing polymer composite deposition. Compos B Eng 2019;177:107284. https://doi.org/10.1016/j.compositesb.2019.107284.
[71] Wang Z, Smith DE. A fully coupled simulation of planar deposition flow and fiber orientation in polymer composites additive manufacturing. Materials 2021;14.

https://doi.org/10.3390/ma14102596.

[72] Bertevas E, Férec J, Khoo BC, Ausias G, Phan-Thien N. Smoothed particle hydrodynamics (SPH) modeling of fiber orientation in a 3D printing process. Physics of Fluids 2018;30. https://doi.org/10.1063/1.5047088.

[73] Ouyang Z, Bertevas E, Parc L, Khoo BC, Phan-Thien N, Férec J, et al. A smoothed particle hydrodynamics simulation of fiber-filled composites in a non-isothermal three-dimensional printing process. Physics of Fluids 2019;31. https://doi.org/10.1063/1.5130711.

[74] Ouyang Z, Bertevas E, Wang D, Khoo BC, Férec J, Ausias G, et al. A smoothed particle hydrodynamics study of a non-isothermal and thermally anisotropic fused deposition modeling process for a fiber-filled composite. Physics of Fluids 2020;32. https://doi.org/10.1063/5.0004527.

[75] Wang Z. A numerical study on the predicted fiber orientation of large area extrusion deposition additive manufactured composites. Polym Compos 2022:1–15. https://doi.org/10.1002/pc.26731.

[76] Yang D, Wu K, Wan L, Sheng Y. A particle element approach for modelling the 3d printing process of fibre reinforced polymer composites. Journal of Manufacturing and Materials Processing 2017;1. https://doi.org/10.3390/jmmp1010010.

[77] Imaeda Y, Todoroki A, Matsuzaki R, Ueda M, Hirano Y. Modified moving particle semi-implicit method for 3D print process simulations of short carbon fiber/polyamide-6 composites. Composites Part C: Open Access 2021;6:100195. https://doi.org/10.1016/j.jcomc.2021.100195.

[78] Folgar F, Tucker III CL. Orientation behavior of fibers in concentrated suspensions. Journal of Reinforced Plastics and Composites 1984;3:98–119. https://doi.org/10.1177/073168448400300201.

[79] Struzziero G, Barbezat M, Skordos AA. Consolidation of continuous fibre reinforced composites in additive processes: A review. Addit Manuf 2021;48. https://doi.org/10.1016/j.addma.2021.102458.

[80] Han N, Cheng J, Yang J, Liu Y, Huang W. Design and implementation of 3D printing system for continuous CFRP composites. MATEC Web of Conferences, vol. 213, EDP Sciences; 2018. https://doi.org/10.1051/matecconf/201821301011.

[81] Albrecht H, Savandaiah C, Löw-Baselli B, Lepschi A, Haider A. Parametric study in co-extrusion-based additive manufacturing of continuous fiber-reinforced plastic. II International Conference on Simulation for Additive Manufacturing -Sim-AM 201, 2019. https://doi.org/10.5281/zenodo.4314900.

[82] Ding X, He Q, Yang Q, Wang S, Chen K. Numerical Simulation of Impregnation Process of Reactive Injection Pultrusion for Glass Fiber/PA6 Composites. Polymers (Basel) 2022;14. https://doi.org/10.3390/polym14040666.

[83] Kobayashi S, Tsukada T, Morimoto T. Resin impregnation behavior in carbon fiber

reinforced polyamide 6 composite: Effects of yarn thickness, fabric lamination and sizing agent. Compos Part A Appl Sci Manuf 2017;101:283–9. https://doi.org/10.1016/j.compositesa.2017.06.030.

[84] Koubaa S, le Corre S, Burtin C. Thermoplastic pultrusion process: Modeling and optimal conditions for fibers impregnation. Journal of Reinforced Plastics and Composites 2013;32:1285–94. https://doi.org/10.1177/0731684413489851.

[85] Ngo SI, Lim Y il, Hahn MH, Jung J. Prediction of degree of impregnation in thermoplastic unidirectional carbon fiber prepreg by multi-scale computational fluid dynamics. Chem Eng Sci 2018;185:64–75. https://doi.org/10.1016/j.ces.2018.04.010.

[86] Thien NP, Tanner RI. A new constitutive equation derived from network theory. J Nonnewton Fluid Mech 1977;2:353–65. https://doi.org/10.1016/0377-0257(77)80021-9.

[87] Ferrás LL, Morgado ML, Rebelo M, McKinley GH, Afonso AM. A generalised Phan–Thien—Tanner model. J Nonnewton Fluid Mech 2019;269:88–99. https://doi.org/10.1016/j.jnnfm.2019.06.001.

[88] Mitsoulis E. 50 Years of the K-BKZ Constitutive Relation for Polymers. ISRN Polymer Science 2013;2013:1–22. https://doi.org/10.1155/2013/952379.